IEEE Access
Multidisciplinary | Rapid Review | Open Access Journal

Received 23 February 2024, accepted 18 March 2024, date of publication 25 March 2024, date of current version 2 April 2024.

Digital Object Identifier 10.1109/ACCESS.2024.3381784

RESEARCH ARTICLE

Battery-Less NFC Conductivity Sensor for Bovine Mastitis Detection in Farming 4.0

ANTONIO LAZARO[1], (Senior Member, IEEE), RAMON VILLARINO[1], MERCE PACIOS[1], MARC LAZARO[1], NICOLAU CANELLAS[1], DAVID GIRBAU[1], (Senior Member, IEEE), AND BEATRIZ PRIETO-SIMON[2,3]

[1]Department of Electronics, Electrics and Automatic Control Engineering, Rovira i Virgili University, 43007 Tarragona, Spain
[2]Institute of Chemical Research of Catalonia (ICIQ), The Barcelona Institute of Science and Technology (BIST), 43007 Tarragona, Spain
[3]ICREA, 08010 Barcelona, Spain

Corresponding author: Antonio Lazaro (antonioramon.lazaro@urv.cat)

This work was supported in part by the Ministerio de Ciencia, Innovacion y Universidades (MICIU)/Agencia Estatal de Inveestigacion (AEI)/10.13039/501100011033/Fondo Europeo de Desarrollo Regional (FEDER), the Union Europea (UE), under Project PID2021-122399OB-I00; in part by MICIU/AEI/10.13039/501100011033/European Union NextGenerationEU/Plan de Recuperacion, Transformacion y Resilencia (PRTR) under Project TED2021-130307B-I00; and in part by Grant PRE2019-089028.

ABSTRACT This work proposes a battery-less Near-Field Communication (NFC) milk conductivity sensor for the early-stage detection of bovine mastitis. A proof-of-concept prototype is designed, which is composed of a loop antenna, an NFC microchip, a microcontroller, a custom conductivity sensor and a temperature sensor. A mobile phone is used as a reader, which additionally provides energy to the sensor to power all the electronic components. Since milk conductivity is temperature-dependent, it is also important to measure the temperature. The prototype has a precision better than 2%, which is similar to that of commercial hand-held conductivity meters. Measurements of the conductivity of cows' milk are made to establish limits that allow healthy cows to be discriminated from those suffering from clinical or subclinical mastitis. To this end, the obtained results are analyzed through ANOVA. The reliability of the method can be improved when milk samples from each quarter are used in the classification. This low-cost device has great potential to be used as on-farm screening tool for the quick identification of bovine mastitis.

INDEX TERMS Near-field communication, battery-less, mastitis detection, conductivity meter, farm 4.0.

I. INTRODUCTION

Terms such as precision livestock farming (PLF), precision agriculture (PA), smart farming, agriculture 4.0, and industry 4.0 are more and more widespread [1]. Smart Farming (also known as Agriculture 4.0, Farming 4.0 or Digital Farming) describes the application of information and data technologies to optimize systems and processes in agriculture and livestock [2]. Precision livestock farming (PLF) and the integration of digital technology will become the most influential trends in the sector, as a growing number of farmers begin to adopt digital technologies to run their businesses [3]. Mastitis is an infectious disease, mostly caused by bacteria, that affects mammary glands. Milk quality in cows is directly tied to the health of the mammary gland (Fig. 1). Therefore, mastitis is one of the diseases causing major economic burden to the dairy industry [4]. It directly impacts on milk quality, reducing its production, and increasing veterinary treatments and expenses on the farm.

Bovine mastitis can be classified into two main types: 1) sub-clinical mastitis, where no visible symptoms can be observed, and 2) clinical, which manifests itself with visible symptoms such as red, swollen, and painful udder, as well as changes in the color and smell of the milk. Somatic cell count (SCC) is applied as an indicator of bovine udder inflammation, and thus is commonly used to confirm mammary infection. SCC levels have been set to classify animals within a healthy group (<200,000 cell/mL), sub-clinical mastitis group (from 200,000 to 500,000 cells/mL) and clinical mastitis group (>500,000 cell/mL). Subclinical mastitis (SCM) can also be considered as the early stage of

The associate editor coordinating the review of this manuscript and approving it for publication was Siddharth Tallur.

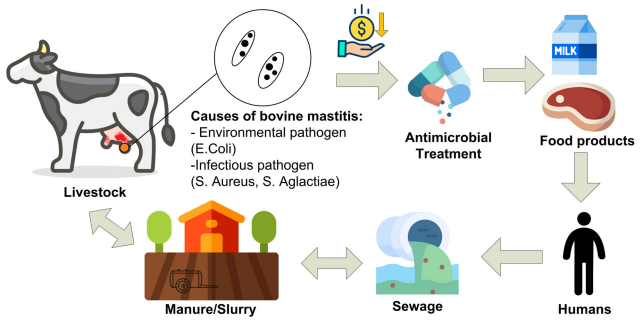

FIGURE 1. Mastitis origin and increase of resistance due to treatment using antibiotics.

a developing infection. The infection is present and causes problems within the udder, but not enough to be noticeable. It also does not cause pain or inflammation of the udder. Clinical mastitis occurs when subclinical mastitis has not been treated in time and becomes now noticeable; in addition, clinical mastitis produces changes in milk quality. Mastitis is a widespread disease throughout the world in both cows and buffaloes. It can pose a high risk in the first two months of lactation. The disease is often transmitted from infected udders to others by environmental contamination, by contact from the milking machine or even by manual milking of other infected cows. Therefore, the management, control and prevention of bovine mastitis that allows early detection before the first symptoms appear, limits the spread of infection and improves the health and welfare of animals, are essential for dairy farms. As a result, it is expected to reduce the use of antibiotics, minimizing their impact on the environment and the emergence of antibiotic resistance (Fig. 1). The severity of the infection affects the metabolism of the mammary cells in cows, significantly impacting on milk quality. The disruption of epithelial cells or enzymatic activity can lead to a decrease in the levels of potassium, the main protein in milk, casein, or to an increase in the levels of lactoferrin. Therefore, early diagnosis of mastitis in cows is of great importance to reduce or prevent production losses associated with the disease. None of the methods used in the laboratory for the diagnosis of bovine mastitis, namely bacterial culturing, and Polymerase chain reaction (PCR), can be easily implemented on-farm. As a result, the on-farm diagnosis of subclinical mastitis commonly relies on the visual observation of the udder and milk. On the other hand, the diagnosis of subclinical mastitis is more complicated because both the milk and the udder do not show evidence of abnormality, although there are nevertheless a high number of somatic cells [5]. Diagnosis of clinical mastitis is commonly based on local and systemic reactions or on milk changes. On the other hand, the diagnosis of subclinical mastitis is more complicated because both the milk and the udder do not show evidence of abnormality. In this case, methods such as those based on measuring SCC are used, as the increase in SCC correlates well with the presence of the infection [5].

Indeed, according to the guidelines given by the International Dairy Federation, the diagnosis of mastitis is mainly based on somatic cell count and bacteriological culture. In this context, measuring the electrical conductivity (EC) of milk is used as an alternative indicator because this parameter changes during mammary gland inflammation. In fact, during mastitis, the blood-milk barrier is damaged and, consequently, the tight junctions between the secretory cells become permeable. As a result, added to the transfer of immune cells and factors from blood to milk, other soluble blood constituents, such as ions, are transferred. In the milk of healthy cows, Na^+ and Cl^- concentrations are lower than those in blood, while K^+ concentrations are higher than in blood. These ion concentrations are tightly controlled by active transport mechanisms of the epithelial cells. However, when the blood-milk barrier is affected, ions can freely move between blood and milk. As a result, Na^+ and $Cl-$ levels in milk increase, while K^+ levels decrease. The outcome is a net increase of the electrical conductivity of milk from the infected quarter [6]. For this reason, EC is considered a reliable indicator for early diagnosis of mastitis in dairy cattle [7], [8].

Compared to other indicators such as SCC and lactate dehydrogenase (LDH) activity that require laboratory facilities and qualified personnel, EC measurements can be potentially performed installing the appropriate device on the milking machine. A main IoT technology used in Farming 4.0 is radio frequency identification Technology. RFID tags contribute to traceability in the livestock supply chain by providing information on the origin, health history, and other relevant details of each animal [9]. Near-field communication (NFC) technology is a type of Radio Identification (RFID) that operates at 13.56 MHz band. The use of NFC technology has grown in recent years for payment applications. Consequently, today most smartphones incorporate NFC readers. There are commercially-available NFC integrated circuits (IC) that harvest radio frequency energy from the reader to acquire and transmit data from sensors to a smartphone over a short distance. As a result, various battery-less NFC-based sensors have been proposed in the literature for several applications [10], [11], [12] including biomedical ones [13], [14], [15], [16]. These NFC sensors readable from smartphones can be of great benefit in the Internet of Things (IoT) paradigm thanks to the ease of accessing the data cloud, identifying an object, obtaining its location or sensing physical or biological parameters.

This paper proposes a battery-less NFC sensor based on conductivity measurements to confirm the diagnosis of bovine mastitis. A smartphone powers the sensor through energy harvesting as well as reads information from the latter. The proposed solution is proven to be effective as a detection technique and is especially suitable for small farms where the cost of implementing an automated monitoring system can be prohibitive. The paper is organized as follows. Section II proposes a low-power method for the measurement of the electrical conductivity. Some methods proposed in

TABLE 1. Cell conductivity constant as a function of the cell geometry.

Geometry	Cell factor constant k
Parallel plates	$d/(W \cdot L)$
Coaxial	$ln(b/a)/(2\pi L)$
Parallel cylinders	$\frac{1}{2\pi L} ch^{-1}\left(\frac{d}{2a}\right)$

the literature are also discussed. Section III describes the proposed NFC system based on a low-power circuit to measure conductivity. At the end of this section, antenna design and tag tuning are described. Experimental results are shown in section IV. Finally, conclusions are provided in section V.

II. CONDUCTVITY: THEORETICAL BACKGROUND

The electrical conductivity of a solution is a measure of its ability to conduct electricity. It directly depends on the concentration of ions in the solution. Electrical conductivity is a measure of the total concentration of dissolved salts in a solution. In addition to using conductivity measurements as an indicator of mastitis, these measurements can provide useful information to other applications such as water treatment, aquaculture, and agriculture. The main methods used to measure EC include inter-electrode conductivity, electromagnetic conductivity, and ultrasonic measurements [17]. The last two methods are usually restricted to measure highly-conductive solutions. Inter-electrode conductivity measurement method is based on the principle of electrolytic conductivity. The conductivity is extracted from the conductance measurement using a probe or conductivity cell. The conductivity σ can be obtained from the measured conductance G using the cell constant k [18]:

$$\sigma = k \cdot G \tag{1}$$

Most low-cost conductivity meters use a two-electrode cell. The cell constant can be derived for simple structures such as transmission lines [19] where the distributed conductance by unit length (G') is proportional to the capacitance per unit length (C') between conductors [20]:

$$G'/C' = \sigma/\epsilon \tag{2}$$

where ϵ is the permittivity. Using this relationship, the cell constant can be calculated from the expressions in Table 1, for the case of structures like the one mentioned and other simple ones represented in Fig. 2. However, a correction term must be added to simple analytical formulas to consider fringing effects [21]. This correction term is introduced by replacing the probe length with an effective probe length calculated as $L_e = L + \Delta L$. Where ΔL can be determined experimentally using two probes with two different lengths. Another method is to use a calibration solution of known conductivity. The cell constant is derived from 1. Despite the necessary calibration, the analytical expressions in Table 1 can serve as a starting point for custom probe design. Conductivity measurements depend on temperature [22]. As the temperature increases, the conductivity increases

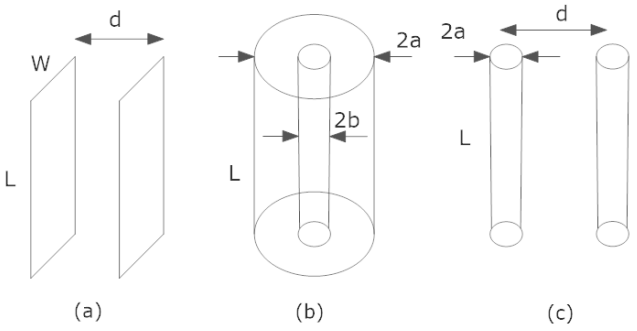

FIGURE 2. Geometry of the probes: (a) Parallel plates, (b) Coaxial, (c) Parallel cylinders.

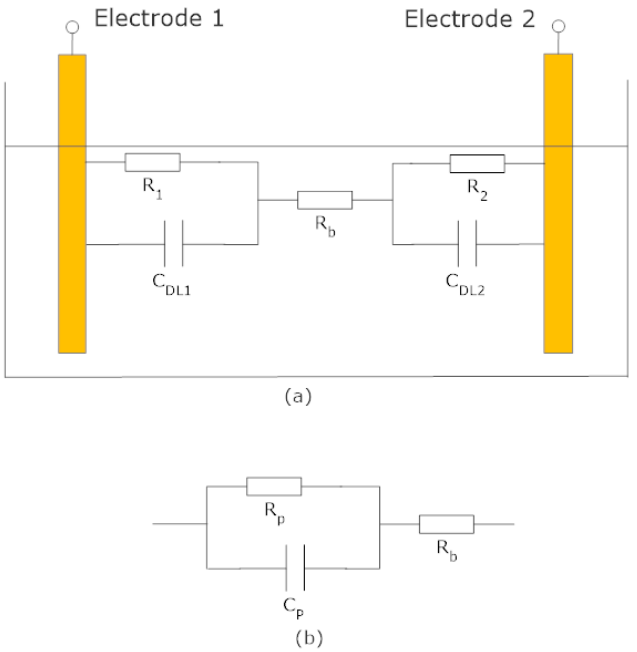

FIGURE 3. (a) Equivalent circuit of conductance cell, and (b) simplified model.

because the viscosity of the solution is reduced, and the movement of the ions is accelerated under the electric field. For this reason, the reading of most conductivity meters is often referenced to a specific temperature, usually $T_0 = 25^{\circ}$C. The degree to which temperature affects conductivity depends on the solution and can be calculated using the following linear equation [23], [24]:

$$\sigma(T) = \sigma_0 \left(1 + \alpha(T - T_0)\right) \tag{3}$$

where $\sigma(T)$ is the conductivity at a temperature T, $\sigma_0 = \sigma(T_0)$ is the conductivity at the calibration temperature T_0, and α is the temperature coefficient of the solution at T_0. To determine the α coefficient of a solution, the conductance is measured over a range of temperatures, and the slope of the linear fitting corresponds to the α coefficient. The impedance of a conductance cell depends on the frequency and can be modeled from an equivalent

circuit. The impedances of this circuit are the ones associated with the interface created by the two electrodes, and the resistance of the bulk solution, R_b (Fig.3). An electrical double layer exists on the interface between the electrode and its surrounding electrolyte. This double layer is formed when ions with charge opposite to that of the electrode are electrostatically attracted. The space between the charged electrode and the charged ions is often on the order of angstroms [25]. These charges separated by a thin insulating layer behave like a capacitor. Thus, the interface between the electrode and the electrolyte is modeled as a double-layer capacitance C_p, in parallel with the faradaic impedance. The faradaic impedance is composed by two terms in series: the polarization resistance or charge-transfer resistance (also known as faradaic resistance) and the Warburg impedance [26]. Warburg impedance models the diffusion (that arises from the mass transfer) process, and can be neglected at high frequencies. Therefore, for the purpose of this work, the faradaic impedance can be modeled using only a polarization resistance. In Figure 3, R_1 and R_2 are the polarization resistances of each electrode, and C_{DL1} and C_{DL2} are the double-layer capacitance at each electrode [27]. The lead resistance is usually small and the parasitic capacitance between electrodes has been omitted in this schema. A simplified equivalent circuit can be obtained by grouping the polarization impedance resulting in the Randle's equivalent circuit (see Fig.3b). The objective is to obtain the conductance associated to the bulk solution $(1/R_b)$ without incorporating any effects caused by the electrodes. Measurement using an external DC potential applied to the conductance cell produces some undesired effects such as electrolysis. Therefore, the excitation must be at AC. To minimize the problems associated with the effect of polarization that increases the electrode resistance, a bipolar pulse of voltage will be applied to measure EC without any flowing net DC current through the solution. If the conductance cell is polarized with a low-amplitude AC voltage (<1 V), the faradaic resistance increases relative to the double-layer capacitance, helping to reduce the effect of polarization. C_{DL1} and C_{DL2} can be increased by increasing the effective surface area with black spongy platinum coating. Consequently, the excitation frequency must be higher than the cut-off frequency f_c to avoid effect of the capacitance on the measurement, and thus obtain R_b. Therefore, in this situation, the conductance (real part of the admittance) remains constant:

$$f_c = \frac{1}{2\pi C_p R_p \cdot R_b/(R_p + R_b)} \tag{4}$$

In practice, frequency values between 1 kHz and 5 kHz considerably reduce the electrolytic saturation [28]. On the other hand, high-frequency values must be avoided to minimize the effect of the capacitance in parallel with the resistance of the electrolytic solution (R_b). Another technique to reduce the effects of polarization is the use of a four-wire resistance measurement [29], which is based on the use of

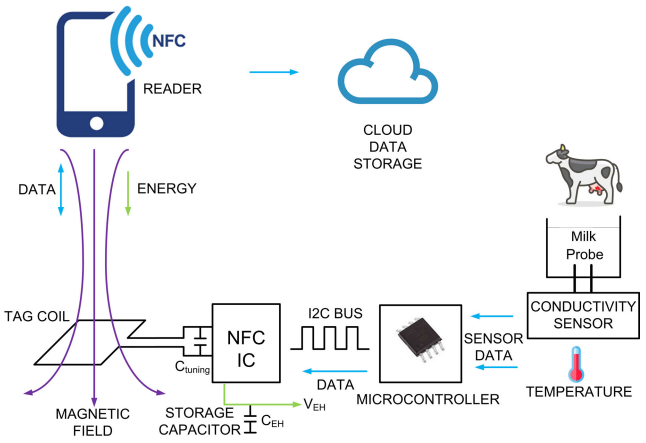

FIGURE 4. Block diagram of the battery-less conductivity meter.

conductivity probes made up of four electrodes. In the four-electrode conductivity measurement, the meter injects current between the outer electrodes and measures the voltage drop caused by the resistance of the electrolyte between the inner electrodes. In the case of measuring conductivity, it is not the wire resistance the one to suppress as in the classical four-wire resistance-measuring method, but rather the added resistance caused by polarization. By using four electrodes instead of two, we can measure the voltage difference across the solution, and completely ignore the resistive effects of electrode fouling. Additionally, a four-electrode sensor has a considerably wider dynamic range than a two-electrode sensor. However, the use of a four-electrode probe increases the cost of the conductivity meters and thus it is not considered in this work.

III. SYSTEM OVERVIEW

The battery-less conductivity meter designed is integrated in a tag. It consists of an NFC IC with energy harvesting capability, the NFC antenna, a microcontroller, a custom conductivity sensor, a temperature sensor to correct the effects of the temperature on the conductivity, and a probe made of two electrodes. The NFC IC is the ST25DV04K from STMicroelectronics. It complies with the ISO/IEC 15693 standard or NFC forum type 5, which defines the modulation parameters, and has energy harvesting capability. The authors have reported in [30] that the chip can supply up to 3 V and 3 mA unregulated depending on the load, using a square-shaped printed loop with dimensions of up to 3 cm on each side. An overview of the proposed system is shown in Fig. 4. Most modern smartphones are equipped with NFC and are used as readers in this work. Therefore, no additional specialized readers are needed, unlike what would happen if UHF RFID was used, reducing the overall cost of the system. When the smartphone detects the presence of a NFC tag in the vicinity, it interrogates it. The NFC tag collects the energy from the magnetic field at 13.56 MHz ISM band to wake-up and bias the internal NFC IC, and external components (such

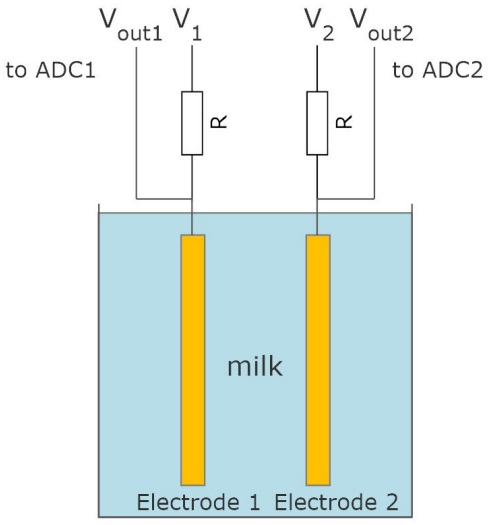

FIGURE 5. Scheme of the conductivity sensor based on two-electrode probes and two resistors.

as sensors and microcontroller) are powered up through the energy harvesting voltage output of the NFC IC, making it is possible to design low-consumption battery-less sensors powered wirelessly from the smartphone. The data is saved in the internal NFC memory and is read using the NFC protocol by load modulation of the antenna using a sub-carrier. In this work, as a proof of concept, an 8-bit microcontroller with 16 kB Flash memory and a 10-bit analog-to-digital converter (ADC) is used (ATTiny1614 from Microchip). It is powered by a 2.5 V low dropout regulator (LMS5214IMG-2.5 from Texas Instruments) connected to the NFC IC energy harvesting output. When the ADC is active, the current consumption at 1 MHz is about 600 μA which can be powered by the NFC. The microcontroller is responsible for measuring the conductivity and temperature, performs the temperature corrections, and saves data to the electrically erasable programmable read-only memory (EEPROM) of the NFC IC through the two-wire inter-integrated circuit (I^2C) serial interface. Data is encoded in a standard NFC data exchange format (NDEF) to be readable via the NFC protocol from standard applications. The firmware for the microcontroller is downloaded using a unified program and debug interface (UPDI) from Arduino IDE. Data can be uploaded from the smartphone to the cloud to monitor, store and further process the measurements. The prototype is manufactured using standard 0.8 mm thick FR4 printed circuit board (PCB), with relative permittivity 4.7 and loss tangent ($tan\delta$) 0.02. The copper metal layer has a thickness of 35 μm (conductivity $\sigma = 4.7 \cdot 10^6$ S/m). Figure 6 shows a circuit diagram of the tag.

According to the equivalent circuit depicted in Fig. 3, the impedance of the cell can be approximated by R_b at high frequency, determining its value from the proposed circuit. The terminals V_1 and V_2 connected to two of the digital outputs of the microcontroller switch every half period ($T/2$)

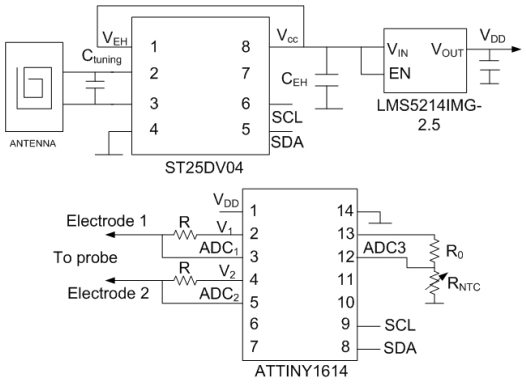

FIGURE 6. Scheme of the tag.

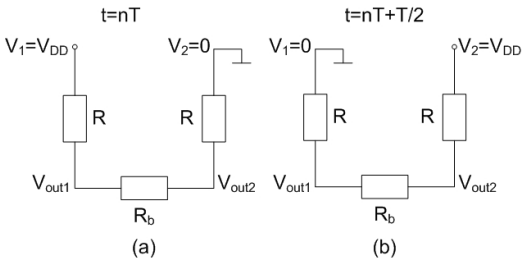

FIGURE 7. Equivalent circuit for each half-period of bipolar square waveform excitation: (a) at t=nT, and (b) t=nT*T/2.

between 0 and the power supply voltage V_{DD}, in order to excite the electrodes by means of bipolar pulses applied to minimize the effect of polarization (see the schema shown in Fig. 5 and the chronogram in Fig. 8). Figure 7 shows the equivalent circuit for each half-period. The output voltage (V_{out1} and V_{out2}) at each half-period can be obtained by analyzing the circuit of Fig. 7:

$$V_{out1}(nT) = \frac{2R}{R_b + 2R} \cdot V_{DD} \tag{5}$$

$$V_{out2}(nT) = \frac{R + R_b}{R_b + 2R} \cdot V_{DD} \tag{6}$$

$$V_{out1}(nT + T/2) = \frac{R + R_b}{R_b + 2R} \cdot V_{DD} \tag{7}$$

$$V_{out2}(nT + T/2) = \frac{2R}{R_b + 2R} \cdot V_{DD} \tag{8}$$

It can be observed from the chronogram and from the equations (5)–(8) that the average or DC voltage difference between both electrodes is zero. The voltage of each of the electrodes (V_{out1} and V_{out2}) is measured by the analog-to-digital converters of the microcontroller. From (5)–(8), the bulk solution resistance is obtained from either a positive or negative pulse using:

$$R_b = \frac{2R}{\frac{V_{DD}}{\Delta V_{avg}} - 1} \tag{9}$$

where ΔV_{avg} is the average voltage difference between the two electrodes at the beginning ($t = nT$) and the end

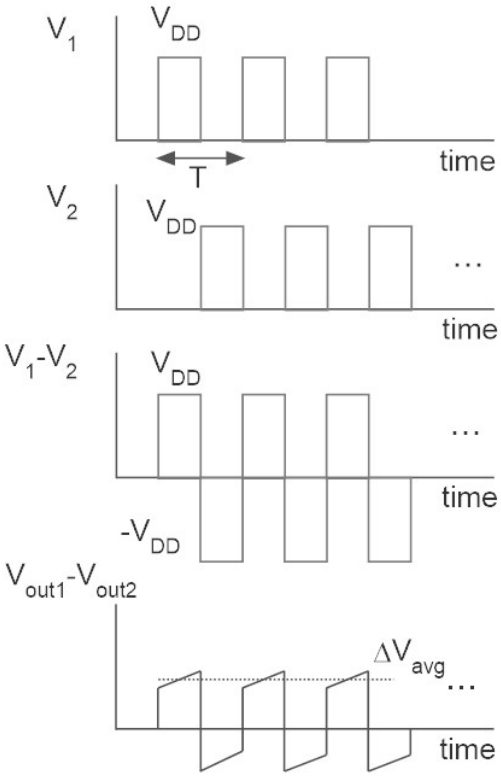

FIGURE 8. Voltage chronogram at the input and output of the conductivity sensor.

$(t = nT + T/2)$ of the pulse (Fig. 8):

$$\Delta V_{avg} = \frac{1}{2}(V_{out1}(nT) - V_{out2}(nT)) + \frac{1}{2}(V_{out1}(nT + T/2) - V_{out2}(nT + T/2)) \quad (10)$$

When performing this averaging, it is observed that the error due to the charge and discharge associated with the capacitive part of the impedance is compensated. Finally, to reduce noise, averaging of several pulses (typically 8 to 32) is performed. A value of R equal to 1000 Ω has been chosen to limit the drop voltage between the electrodes below 1 V and avoid an excessive current consumption in the voltage divider. The proposed method is simple and requires low-power compared to the classical method based on oscillators and transimpedance amplifiers, and subsequent detection by full-wave detectors [31], which are based on operational amplifiers (see, for example, the schematic used in the EC meter commercialized by Seed Studio [32]). Compared to other methods proposed in [33] and [34] based on impedance measurements, the proposed method in this work does not need as many active components (operational amplifiers), thus reducing the complexity, cost, and current consumption. A negative temperature coefficient (NTC) thermistor connected to a voltage divider (see Fig. 6) is used to determine the temperature of the solution. A 100 kΩ NTC protected with thermal silicone to avoid drawing excessive current and a resistor of 100 kΩ for the voltage divider are chosen. The resistance of the temperature probe (R_{NTC}) is determined from the measurement of the voltage at the output of the divider using another ADC input available in the microcontroller (ADC3):

$$R_{NTC} = \frac{R}{\left(\frac{V_{DD}}{V_{ADC3}} - 1\right)} \quad (11)$$

The temperature is calculated from the NFC thermistor using the Steinhart-Hart equation:

$$\frac{1}{T} = \frac{1}{T_0} + \frac{1}{\beta} ln\left(\frac{R_{NTC}}{R_0}\right) \quad (12)$$

where R_0 is the nominal NTC resistance at the temperature $T_0 = 209$ K and $\beta = 3950$ K^{-1}.

Due to space limitations, smartphones use smaller coils compared to those used by custom NFC readers, there are variations between different phone models, and normally the structure is not optimal for energy harvesting. In addition, the read range of sensor tags is reduced when using energy harvesting compared to those not using it (standard NFC cards without sensing capability). To optimize energy harvesting, one must minimize the load current that must be harvested, and simultaneously try to maximize the power conversion efficiency between the reader and the tag. In this design, the voltage divider used to obtain the conductance (Fig. 5) is the element that requires the highest current consumption, followed by the microcontroller. To reduce the total consumption, a microcontroller frequency of 1 MHz and a supply voltage of 2.5 V are chosen. After the measurement, the data is saved in the NFC IC EEPROM via the I^2C bus. This bus requires pull-up resistors on both the clock (SCL) and data (SDA) lines. Pull-up resistors connected to the NFC energy harvesting output (V_{EH}) of 20 $k\Omega$ are used in the prototype to limit the sink current when either line is pulled down. During the interrogation, the smartphone sends modulated commands to the tag. There are small voltage drops at the output of the internal IC rectifier and, therefore, at the energy harvesting NFC output caused by this modulation. A capacitor C_{EH} connected to the energy harvesting NFC output is used to mitigate the voltage drop during the modulation pauses of the reader because it does not transmit the carrier during the pause period whose duration is T_p. In both standards, ISO 14443-3 and ISO 15693 which are the most used in NFC IC with energy harvesting, T_p is approximately 10 μs. The voltage drop can be calculated from the discharge of the storage capacitor:

$$V_{drop} = \frac{I_L \cdot T_p}{C_{EH}} \quad (13)$$

where I_L is the load current demanded from the energy harvesting output. For a voltage drop of 20 mV at the regulator input, which is tolerable for low-drop regulators and a load current of 2 mA, a minimum storage capacitor of $C_{EH} = 1\mu F$ is needed. The low-drop regulator used in the prototype provides a regulated 2.5 V output from the unregulated 3 V supplied by the NFC IC's energy harvesting

output. It supports a maximum current consumption of 10 μA and has a voltage dropout of 0.2 V. Therefore, it can absorb small voltage drop at the input in case of misalignment between the coils of the reader and the tag or in case of detuning effects.

A. ANTENNA DESIGN AND TAG TUNING

In this proof-of-concept prototype, there is no space limitation, therefore there is a great degree of freedom in the coil design. A spiral-shaped coil with 6 turns and an external diameter of 40 mm has been designed, manufactured on one of the surfaces of the PCB. The width of the traces and the separation between them is 0.7 mm. The value of the inductance is needed to get an initial estimation of the value of the tuning capacitor since it is necessary to adjust the resonance of the tag to 13.56 MHz. The inductance is calculated using the Wheeler's formula [35]):

$$L = K_1 \mu_0 N^2 \frac{D_{av}}{1 + K_2 \rho} \tag{14}$$

where μ_0 is the vacuum magnetic permeability constant ($4\pi \cdot 10^{-7}$ H/m), N is the number of turns. The average diameter D_{av} between the outer diameter D_{out} and inner diameter D_{in} is given by:

$$D_{av} = (D_{out} + D_{in})/2 \tag{15}$$

The fill factor ρ measures the hollowness of the inductor, and it is defined as:

$$\rho = \frac{D_{out} - D_{in}}{D_{out} + D_{in}} \tag{16}$$

In (14), the coefficients K_1 and K_2 for a square-shaped inductor are 2.34 and 2.75, respectively. The quality factor of the inductance can be obtained from the resistance of the wire considering the skin effect [36]. The estimated inductance value and the quality factor obtained are, respectively, 2.06 μH and 134 at 13.56 MHz, values very close to those obtained with the full-wave simulator Keysight Advanced Design System (ADS) using the Momentum method (an inductance of 2.09 μH and a quality factor of 136). Figure 9 compares the simulated and measured inductance and quality factor values, in good agreement with those obtained in the analytical models and simulations. To this end, the inductance and quality factor are obtained from the impedance calculated from the reflection coefficient (S_{11}) of a prototype antenna measured with a VNA. The maximum transfer of energy from the reader to the tag is achieved when the resonance frequency of the tag matches the operation frequency (13.56 MHz). To adjust the resonance frequency, the input impedance of the NFC IC at the antenna terminals is needed, which can be approximated by an IC chip capacitance C_{IC} in parallel with a resistance R_{IC}. Whereas C_{IC} is nearly constant for typical input power ranges and it is provided by the manufacturer (or it can be easily measured with a capacitance meter), the resistance R_{IC} is nonlinear and depends on the input voltage due to the nonlinear behavior of the internal IC rectifier

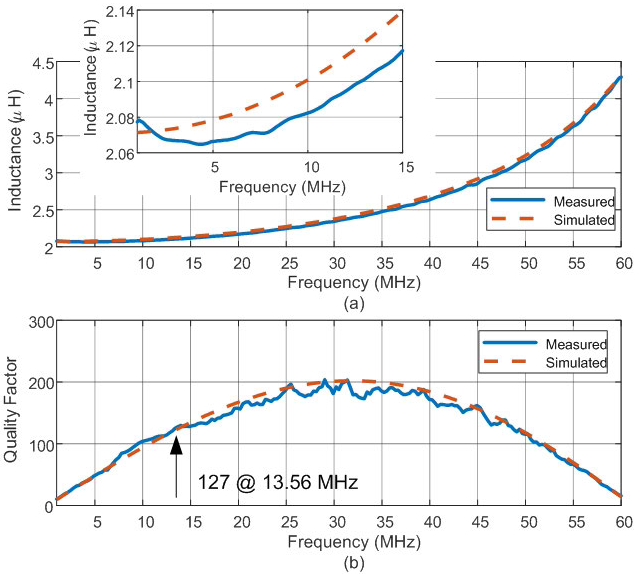

FIGURE 9. Comparison between measurement and simulation of:(a) Measured and simulated antenna inductance (the inset shows a zoom around 13.56 MHz), and (b) quality factor as a function of the frequency.

and the protection limiter at the input of the IC. The IC capacitance for the ST25DV04 is 28.5 pF. The resonance frequency is adjusted by adding a tuning capacitance C_{tuning} connected at the input of the antenna. The tag's resonance frequency f_r is calculated using the following expression:

$$f_r \approx \frac{1}{2\pi\sqrt{L(C_{IC} + C_p + C_{tuning})}} \tag{17}$$

where C_p is the antenna parasitic capacitance (including the interconnections to the IC), which is in the order of a few pF. The size of the antenna is compatible with the typical size of the antennas integrated into modern smartphones. These NFC antennas have sizes of about 2-2.5 cm^2 [37], [38], [39], [40] and are integrated around the camera aperture or over the battery by means of ferrite shields. However, the presence of metallic parts in the smartphone, when approached to the tag it reduces its coil inductance and can produce its detuning. The smartphone antenna usually uses ferrite sheets and is therefore less detuned than the one on the tag. One solution, as proposed in [36] consists in shielding the tag antenna with ferrite as well. Another solution is to adjust the resonance frequency taking into account the reduction of inductance caused by the smartphone assuming a distance between the tag and the smartphone. This adjustment can be easily performed including a spacer in the protection case of the tag that fixes the distance between both. Then, the tuning capacitance is obtained experimentally measuring the resonance frequency with a vector network analyzer (VNA). The measurement is performed from the peak in the reflection coefficient of a test coil located below the tag (at a sufficient distance for the coupling to be weak) and locating a cell phone or a metallic plate that emulates the smartphone on

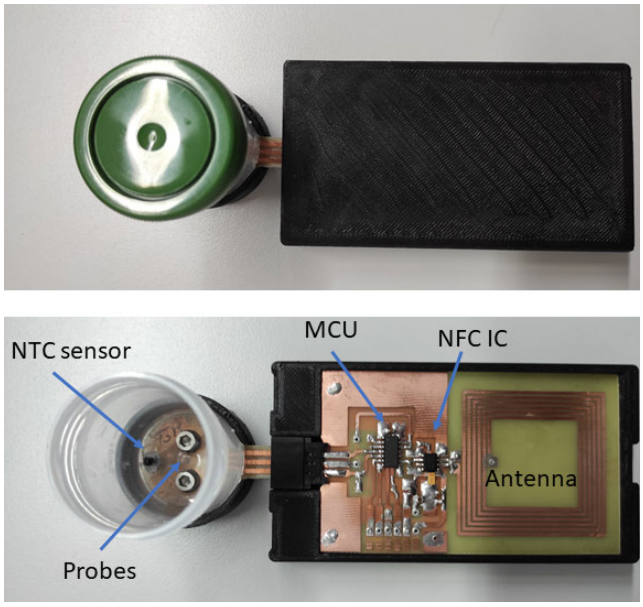

FIGURE 10. Photography of the prototype including the protection box (top view) and PCB board with main components (bottom view).

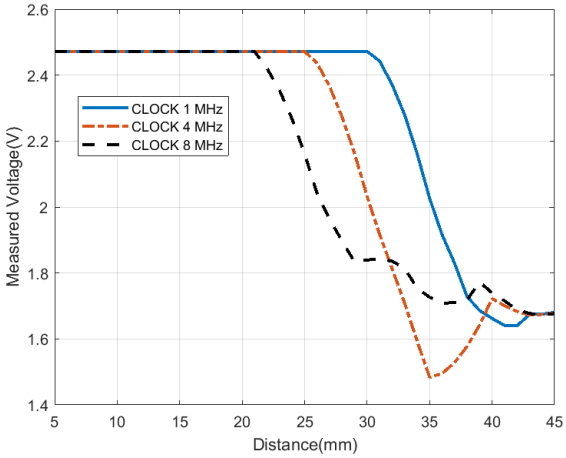

FIGURE 11. Measurement of the regulated voltage as a function of the distance between the tag and the smartphone for different clock frequencies of the microcontroller.

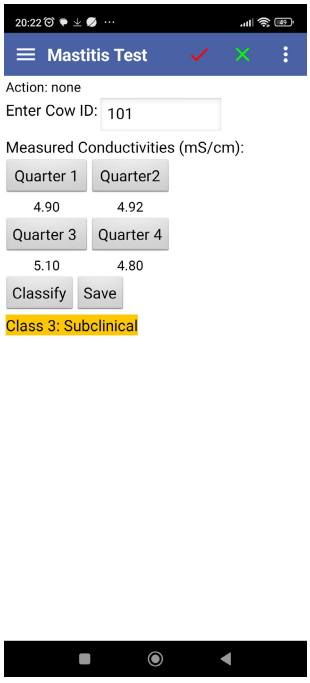

FIGURE 12. Screenshot of the Android application developed to classify the health status of cows using decision rules based on conductivity measurements.

the spacer. In the prototype, the tuning capacitance is 69 pF. The resonance can be adjusted using (17) as starting point to find the tuning capacitance. A great variation in the distance during the measurement can produce an undesired drop of voltage that can affect the sensor measurement. Therefore, in this application, the smartphone is expected to be on top of the tag for the duration of the measurement (few seconds in this work). Such approach also reduces the cost of the device, since the use of ferrite sheets is no longer necessary.

B. PROTOTYPE

Figure 10 shows a photo of the prototype. The temperature sensor and the conductivity probe are integrated into a small removable measuring cell where the milk sample to be analyzed is introduced. The measuring cell can be easily plugged into the main PCB, facilitating its cleaning and replacement. The board that includes the microcontroller (MCU), the NFC chip, the antenna, and the rest of the electronics is protected with a 3D-printed. A microcontroller programming connector is included to save the MCU firmware. The tag can be read by placing the mobile phone on top of it. The energy harvesting range is tested with the setup described in [30]. Figure 11 shows the measured voltage at the output of the regulator as a function of the distance between the NFC reader (smartphone) and the tag. A multimeter connected to a PC is used for the measurements. A Xiaomi Redmi 10 smartphone is used as reader, located on a mobile structure connected to a stepper motor with a linear actuator controlled by a PC, which permits to change the distance between smartphone and tag. The figure shows the measured voltage as a function of the distance for different MCU clock frequencies. It can be concluded that the tag can operate close to 20 mm at 8 MHz and almost 30 mm at 1 MHz. The difference is attributed to the increase of tag current consumption caused by the MCU clock frequency. An Android application (app) has been designed for demonstration purposes. A screenshot is shown in Fig. 12. The app reads the NDEF text saved in the EEPROM of the NFC IC. A measurement can be saved for each quarter. Subsequently, decision rules based on a comparison of the measured conductivity based on a set of threshold levels and the difference conductivity measured among quarters are applied to classify the state of the cow into three different groups: healthy, subclinical or clinical. The measurements

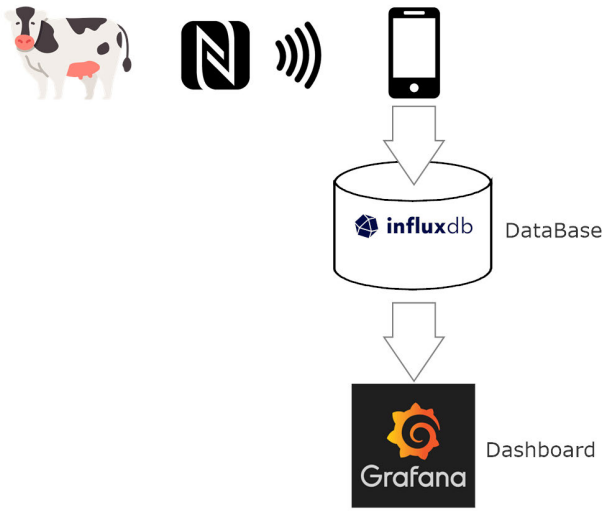

FIGURE 13. Data flow scheme. Data are stored in a database (InfluxDB) and can be visualized with a Grafana-designed dashboard.

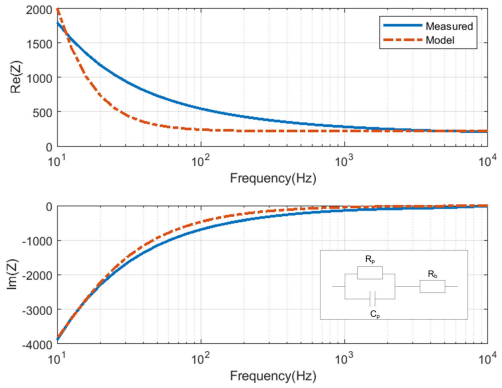

FIGURE 14. Measurement and modeling (Randles equivalent circuit) of the real (top) and imaginary (bottom) part of the impedance of the probe immersed in milk (conductivity 4.7 mS/cm) as a function of frequency.

can be uploaded to a database. In the prototype, an InfuxDB database is selected. A cow identifier is used to identify the cow, and the data is stored in a time series database using a Representational State Transfer Application Programming Interface (REST API) call. The app has various options to configure the database IP and security control. Data can be easily monitored with a dashboard designed with Grafana tool (see Fig. 13).

IV. RESULTS

A. PROTOTYPE VALIDATION.

In order to investigate the frequency behavior of the probes immersed in milk, the impedance between the electrodes is measured by Electrochemical impedance spectroscopy (EIS) using a Palm Sense 4 instrument. A probe consisting of two 3 mm diameter cylinders spaced 10 mm apart and 2.5 mm long is used. Figure 14 shows the measured impedance as a function of frequency between 10 Hz and 10 kHz. The elements of the Randles equivalent circuit obtained upon data fitting are R_b=218.4 Ω, R_p=6140 Ω, and C_p=2.44 μF. Good agreement is obtained at high frequencies (1 kHz to 10 kHz) which is the range of interest. However, other elements such as Warburg impedance must be added to improve the fitting at low frequencies [41]. The imaginary part is negligible compared to the real part for frequencies higher than 1 kHz. Using the obtained Randles equivalent circuit, the response of the sensor as a function of time is simulated for pulse frequencies of 1 kHz and 10 kHz (see Figure 15). The resistance estimated from the simulations is 219.4 Ω at 1 KHz, and 200.4 Ω at 10 kHz. Pulses of 1 V of amplitude and R=1 $k\Omega$ are used in the simulations. The simulation is performed using the Keysight ADS circuit simulator in transient mode obtaining a good agreement with the measured resistance of 219.0 Ω at 1 kHz. These values are very close to the fitted value of R_b of 218.4 Ω. From these results, it can be concluded that a frequency around 1 kHz must be used, so that the effect of the capacitance can be compensated with the proposed method.

Figure 16 compares the conductance measured with an impedance meter (Keysight model U1731C) measuring the resistance at 1 kHz and the proposed method for a probe with cell constant 1 cm^{-1} for saline (NaCl) aqueous solutions at different concentrations (the conductivity is measured with a commercial Hanna conductivity meter). There is good agreement between the conductance values obtained in the desired range. The error between the two systems is less than 3% between 4 and 6 mS/cm, which is the expected conductivity range in the milk. Figure 17 shows an example of measurement of the voltage at the probes using an oscilloscope. The system is powered by the smartphone and a sample of milk with 4.4 mS/cm is tested. The system shows a similar behavior to that predicted by the simulations. In this case, a frequency of 2 KHz pulse is used and the microcontroller clock is set at 4 MHz. Since the temperature can vary from one sample to another, milk conductivity results are shown in Figure 18 as a function of temperature. The conductivity presents a linear behavior, as described by (3). The temperature is measured with an NTC sensor and its slope coefficient ($\alpha = 0.01631$/K) is obtained by linear regression. The value obtained for the slope coefficient is close to that recommended for the 0.01 M KCl solution given in [42]. The repeatability of measurements between different sensors is studied. For this purpose, 4 sensors with their respective probes have been made. It has been observed that these sensors, using an average value of the calibration constant cell k (see (1)), present variations in the measured conductivity of the order of 5%. These are mainly due to the mechanical manufacturing tolerances of the proposed low-cost probes. To improve the reproducibility, a calibration of the probes is required. To this end, each conductivity cell has been calibrated using a calibration solution with known conductivity. The HI7039L 5 mS/cm conductivity standard from Hanna Instruments has been used (which is close to the typical milk conductivity). The calibration constant is recorded in the firmware of the microcontroller

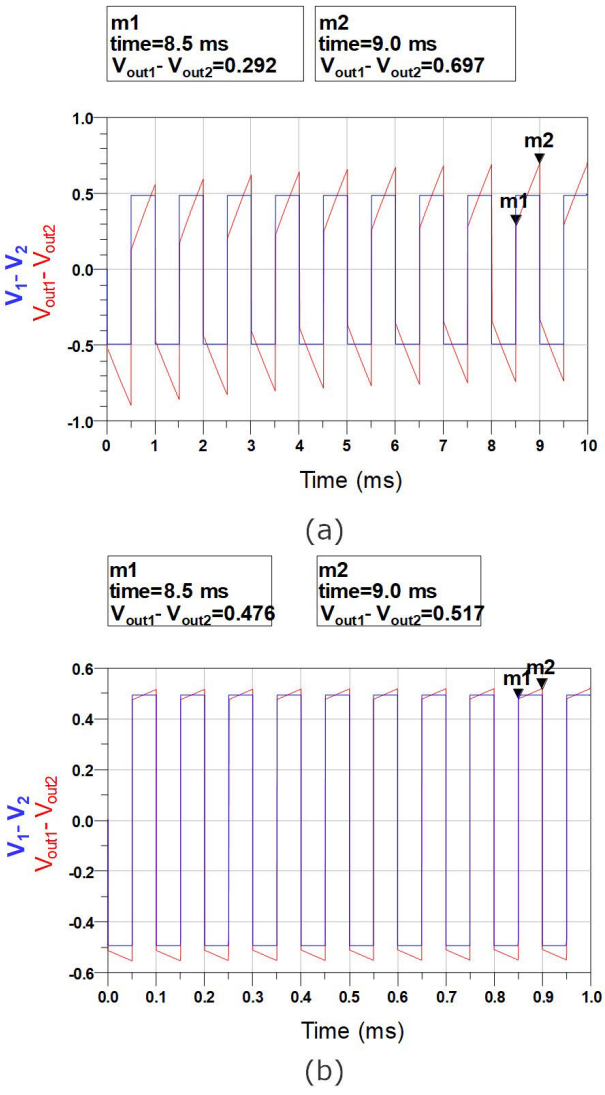

FIGURE 15. Simulation of the response of the sensors at (a) 1 kHz and (b) 10 kHz using the Randles circuit adjusted for milk with conductivity of 4.7 mS/cm.

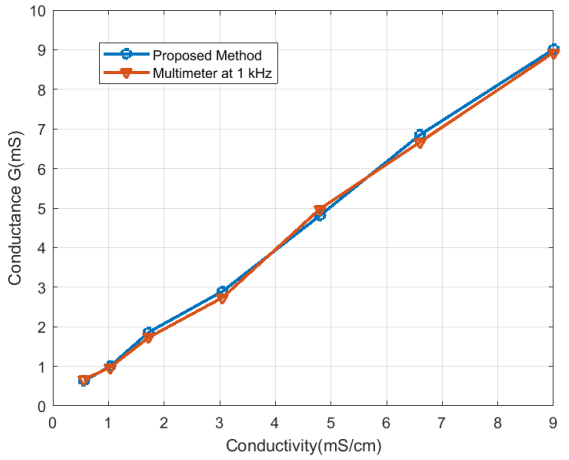

FIGURE 16. Comparison of the measured conductance with a multimeter at 1 kHz and the proposed method as a function of the conductivity of a saline aqueous solution.

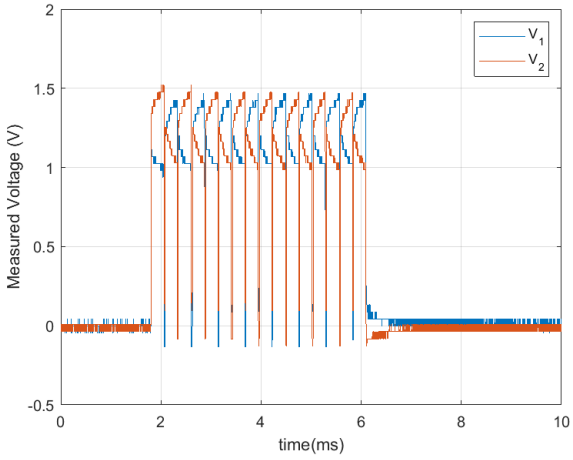

FIGURE 17. Sensor response measured at 2 kHz biased with the NFC for a milk sample with conductivity of 4.4 mS/cm.

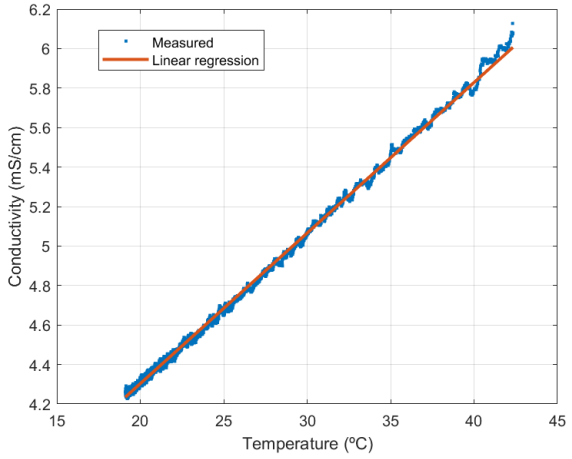

FIGURE 18. Measured conductivity and linear regression as a function of temperature (slope coefficient $\alpha = 0.01631$/K).

and can be updated from the smartphone using a calibration menu in the configuration. The temperature dependence has been assumed linear with the same slope coefficient ($\alpha = 0.01631$/K) for each sensor. Therefore, only a one-point calibration is required. After this calibration, the difference between sensors has been improved notability. Figure 19 shows a boxplot comparing 100 milk samples with a nominal conductivity of 4.5 mS/cm (measured with a commercial Hanna HI 98312 conductivity meter) taken with the smartphone over 10 min. The conductivity for each sample is obtained using (9) and (10), averaging 32 bipolar pulses. The difference in the mean value between the four sensors is reduced to less of 0.013 mS/cm or 0.29% of the nominal value. The deviation from the mean value is associated to measurement noise mainly due to ADC quantization error and power supply noise. Figure 19 shows that the standard deviation is between 1.7% and 2% of the nominal value. This accuracy is comparable to

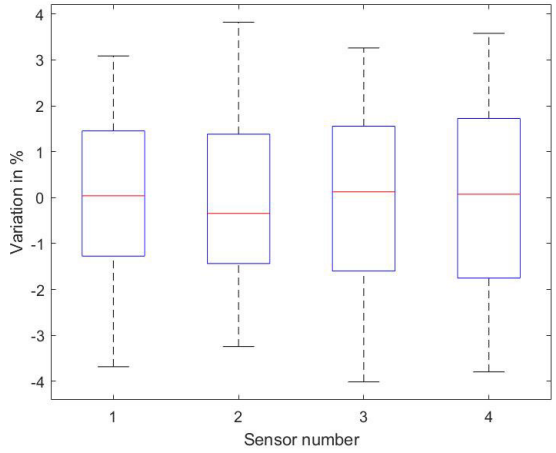

FIGURE 19. Measured conductivity variation in % for the measured 100 samples using four sensors. The red line indicates the mean, and the height of the box its standard deviation. The minimum and maximum deviations between the samples are also indicated for each sensor.

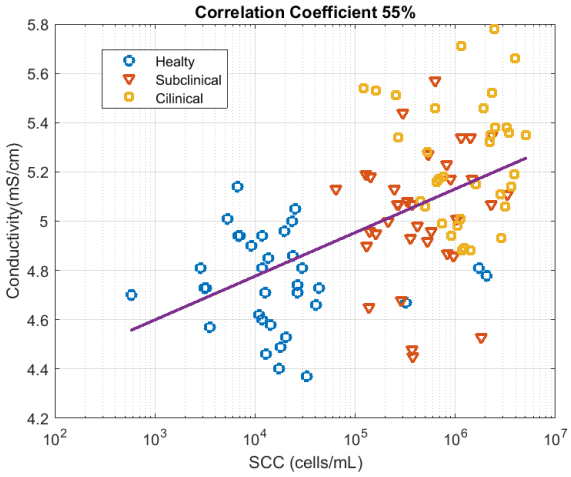

FIGURE 20. Measured conductivity as a function of SCC values (Correlation coefficient 0.55).

the commercial instrument (which is 2% for Hanna HI 98312 conductivity meter).

B. MASTITIS DETECTION.

Next, the feasibility of predicting mastitis infection from milk conductivity measurements is assessed. Somatic cell count (SCC) is used as an indicator of udder health and milk quality and thus is used here to validate the possibility to confirm mastitis infection via milk conductivity measurements. From a heard of Holstein Friesian cattle, 15 cows are selected and divided in three groups of five cows each, healthy animals, animals with subclinical mastitis, and animals with clinical mastitis, according to SCC levels measured during three consecutive days (healthy animals, <200,000 cells/mL; animals with subclinical mastitis, 200,000-500,000 cells/mL; animals with clinical mastitis, >500,000 cells/mL). Then, milk samples from the four quarters of each cow are collected

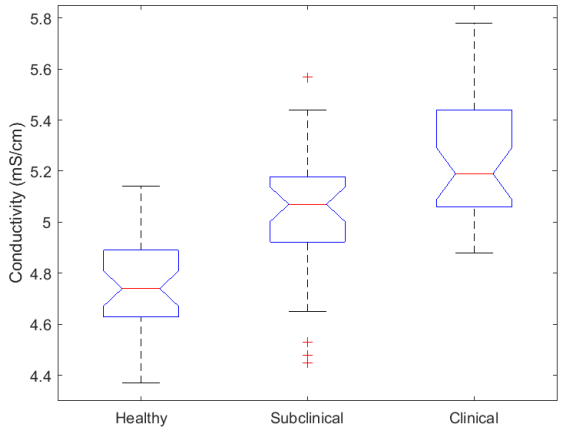

FIGURE 21. Anova Test to assess the significance of the variance between the means of conductivity calculated for milk samples from healthy animals, animals with subclinical mastitis, and animals with clinical mastitis.

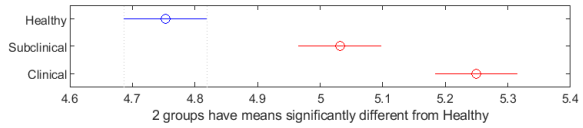

FIGURE 22. Mean estimates and standard errors for each group class.

in days 4, 5, 6, 7, 10, 12, and 14. In total, 105 samples were collected and their SCC levels tested. All those samples were then used to measure their conductivity. Figure 20 shows the measured conductivity at 25ºC with the proposed system as a function of the number of SCC (cells/mL) on a logarithmic scale. The correlation coefficient between the somatic cell count and the conductivity is close to 55%. Interestingly, the dispersion values observed is higher for clinical and subclinical cases than for healthy cows. The significance of the difference between means is assessed by the analysis of variance (ANOVA) [43]. A one-way ANOVA test is performed to analyze the variance using MATLAB software. Figure 21 shows the box plots of data by group. P-values for the test below 0.05 indicate that the group mean differences are significant. A p-value of $1.4 \cdot 10^{-13}$ is obtained. A multiple comparison test by pairwise comparison to identify the groups that have significantly different means is performed (see Fig. 22). The p-values obtained are $6.2 \cdot 10^{-6}$, $5.3 \cdot 10^{-14}$,$0.47 \cdot 10^{-3}$ for healthy-subclinical, healthy-clinical and subclinical-clinical groups, respectively. In the last figure, the blue circle indicates the mean of the control group. The red circles and bars represent the means and confidence intervals for the groups that have significantly different means from the control group. It can be seen how the red bars do not cross the dotted vertical line that represents the mean of the control group. Groups that do not have significantly different means appear in grey. The figure shows multiple comparisons of the means. By default, the mean healthy milk group is highlighted, while the comparison interval is blue. Because the comparison intervals for the

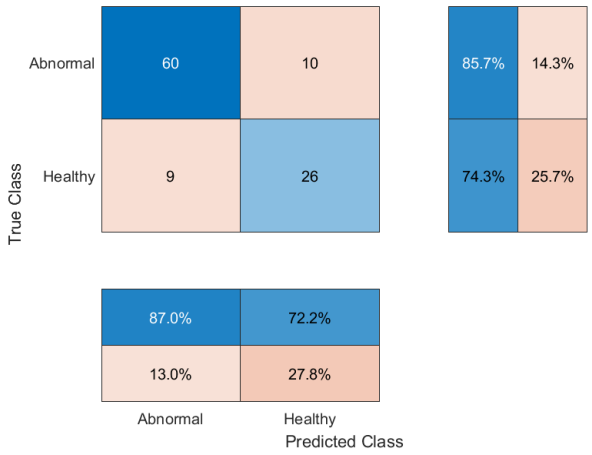

FIGURE 23. Confusion matrix considering two classes: healthy and abnormal or mastitis-infected cows with either subclinical and clinical mastitis.

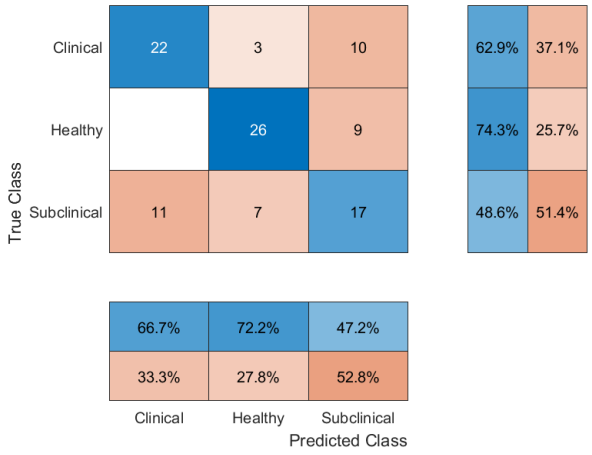

FIGURE 24. Confusion matrix considering three classes: healthy, subclinical, and clinical mastitis-infected cows.

other two groups do not intersect with the intervals for the healthy milk group, they are highlighted in red. This lack of intersection indicates that both means are different from those of the healthy milk group. It can be shown that all group means are significantly different from each other. Based on the mean values of the conductivity a simple classification of the milk samples can be performed. It is considered that the conductivity of healthy milk is below 4.9 mS/cm, that of the subclinical is between 4.9 mS/cm and 5.15 ms/cm and the milk from clinical mastitis-infected cows presents values above 5.15 mS/cm. Considering two classes, milk from healthy and mastitis-infected cows (the latter including milk from cows with either subclinical or clinical mastitis), the confusion matrix is shown in Figure 23. The sensitivity or probability of a positive test given confirming mastitis infection, calculated as the number of true positives over the total number of sick individuals in the population is 85.7%. The specificity or probability of a negative test of a healthy condition, calculated as the number of true negatives over

TABLE 2. Variation of conductivity between quarters as a function of the infection state.

Case	$\Delta\sigma$	$\Delta\sigma/\overline{\sigma}$
Healthy	0.53	11.27%
Subclinical	0.82	16.81%
Clinical	0.92	18.36%

the total number of healthy individuals in the population is 74.29%. Figure 24 shows the confusion matrix between the known and predicted milk groups. This matrix shows that subclinical cases can be confused with both clinical and healthy cases and are therefore more difficult to be detected correctly. Greater reliability could be obtained if differences between quarters of the same cow were considered, thereby allowing for variation between animals in the normal or basal level of these constituents [44]. Table 2 compares the average variation of the conductivity between quarters and the normalized variation with respect to the average conductivity of the quarters for a set of 37 cows. Higher reliability can be obtained by comparing the readings from different quarters [44]. Even with a single test, all severely infected quarters could be detected if one or more were 16% higher than the lowest in that particular animal, or if the level exceeded the conductivity threshold [45]. Therefore, the integration of conductivity sensors in automatic milking machines would allow continuous monitoring of milk conductivity to quickly identify those animals susceptible to be infected, and thus be selected to undergo more sophisticated analysis to confirm mastitis. Furthermore, low-cost solutions such as the one proposed in this work can also be effective as screening techniques, especially on small farms where the cost of implementing an automated monitoring system may be prohibitive.

V. CONCLUSION AND FUTURE WORK

NFC integrated circuits (IC) with energy harvesting capabilities are currently available in the market. The use of these NFC ICs, together with low-power microcontrollers, allows creating battery free and environmentally friendly battery-less NFC sensors for several applications in IoT, since they can be read from smartphones. In this work, the design of a battery-less NFC milk conductivity sensor to be used on farms that allows for rapid evaluation of the state of milk and identification of cows susceptible to be infected with mastitis has been presented. The implementation of this technique as part of a Farm 4.0 concept can help to improve farm productivity and reduce the use of antibiotics thanks to the early identification of animals with mastitis. A proof-of-concept prototype has been integrated into a housing to measure the conductivity of milk, with a precision better than 2%, which is similar to that of commercial hand-held conductivity meters. A smartphone takes the role of powering the sensor electronics to measure data, establishes the communication with the sensor and also uploads the measured data to the cloud to be registered

into a database for analysis over time, all of this managed and displayed through an app. Experimental results have shown good correlation between the measured conductivity and SSC values for 105 milk samples, collected from the four quarters of 15 cows at days 4, 5,6, 7, 10, 12 and 14 from the beginning of the experiment. A classifier based on the comparison of the conductivity with fixed thresholds obtained during a measurement campaign has been proposed. It has been found that the conductivity measured in the milk collected from healthy cows is less than 4.9 mS/cm, that of milk samples from cows with subclinical mastitis is between 4.9 mS/cm and 5.15 mS/cm, and that from the milk of cows with clinical mastitis presents values above 5.15 mS/cm. In the experiments, the sensitivity and the specificity obtained are 85.7% and 74.29%, respectively. The classification of cases with subclinical mastitis is more complex than in the other cases since the milk from cows with subclinical mastitis shows more dispersion in the measured conductivity. For this reason, it has been suggested that, in doubtful cases, each of the quarters should be tested. The analysis of the differences between conductivity measurements of the milk collected from each different quarter can increase the success rate of the classification of cows in healthy and infected groups. Differences greater than 16% can indicate cows are susceptible to be infected with mastitis. The tests proposed in this work have been performed manually and are low cost. This creates ease for farmers, who do not need expert knowledge to perform the test and analyze the results thanks to the smartphone app. In the future, the conductivity sensor developed could be integrated into automatic milking machines to perform automatic and noninvasive measurements of the entire farm population.

ACKNOWLEDGMENT

The authors would like to thank Dr. Lukasz Gontar, Dr. Andzelika Drutowska, and Dr. Maksymilian Kochanski from the Research and Innovation Centre Pro-Akademia, Poland, for the provision of the milk samples used in the study and the analysis of their SCC levels and classification.

REFERENCES

[1] S. Morrone, C. Dimauro, F. Gambella, and M. G. Cappai, "Industry 4.0 and precision livestock farming (PLF): An up to date overview across animal productions," *Sensors*, vol. 22, no. 12, p. 4319, Jun. 2022.

[2] D. Berckmans, "General introduction to precision livestock farming," *Animal Frontiers*, vol. 7, no. 1, pp. 6–11, Jan. 2017.

[3] E. Tullo, A. Finzi, and M. Guarino, "Environmental impact of livestock farming and precision livestock farming as a mitigation strategy," *Sci. Total Environ.*, vol. 650, pp. 2751–2760, Feb. 2019.

[4] H. Hogeveen, K. Huijps, and T. Lam, "Economic aspects of mastitis: New developments," *New Zealand Veterinary J.*, vol. 59, no. 1, pp. 16–23, Jan. 2011, doi: 10.1080/00480169.2011.547165.

[5] N. Sharma, V. Pandey, and N. Sudhan, "Comparison of some indirect screening tests for detection of subclinical mastitis in dairy cows," *Bulgarian J. Veterinary Med.*, vol. 13, no. 2, pp. 98–103, 2010.

[6] B. J. Kitchen, "Bovine mastitis: Milk compositional changes and related diagnostic tests," *J. Dairy Res.*, vol. 48, no. 1, pp. 167–188, Feb. 1981.

[7] E. Norberg, H. Hogeveen, I. R. Korsgaard, N. C. Friggens, K. H. M. N. Sloth, and P. Løvendahl, "Electrical conductivity of milk: Ability to predict mastitis status," *J. Dairy Sci.*, vol. 87, no. 4, pp. 1099–1107, Apr. 2004.

[8] J. Bonestroo, M. van der Voort, N. Fall, U. Emanuelson, I. C. Klaas, and H. Hogeveen, "Estimating the nonlinear association of online somatic cell count, lactate dehydrogenase, and electrical conductivity with milk yield," *J. Dairy Sci.*, vol. 105, no. 4, pp. 3518–3529, Apr. 2022.

[9] S. Silva, J. Araujo, C. Guedes, F. Silva, M. Almeida, and J. Cerqueira, "Precision technologies to address dairy cattle welfare: Focus on lameness, mastitis and body condition," *Animals*, vol. 11, no. 8, p. 2253, Jul. 2021.

[10] J. Morak, H. Kumpusch, D. Hayn, R. Modre-Osprian, and G. Schreier, "Design and evaluation of a telemonitoring concept based on NFC-enabled mobile phones and sensor devices," *IEEE Trans. Inf. Technol. Biomed.*, vol. 16, no. 1, pp. 17–23, Jan. 2012.

[11] A. Lazaro, M. Boada, R. Villarino, and D. Girbau, "Study on the reading of energy-harvested implanted NFC tags using mobile phones," *IEEE Access*, vol. 8, pp. 2200–2221, 2020.

[12] M. Boada, A. Lazaro, R. Villarino, E. Gil-Dolcet, and D. Girbau, "Battery-less NFC bicycle tire pressure sensor based on a force-sensing resistor," *IEEE Access*, vol. 9, pp. 103975–103987, 2021.

[13] A. Lazaro, R. Villarino, and D. Girbau, "A survey of NFC sensors based on energy harvesting for IoT applications," *Sensors*, vol. 18, no. 11, p. 3746, Nov. 2018.

[14] A. Lazaro, R. Villarino, M. Lazaro, N. Canellas, B. Prieto-Simon, and D. Girbau, "Recent advances in batteryless NFC sensors for chemical sensing and biosensing," *Biosensors*, vol. 13, no. 8, p. 775, Jul. 2023. [Online]. Available: https://www.mdpi.com/2079-6374/13/8/775

[15] A. Lazaro, M. Boada, R. Villarino, and D. Girbau, "Battery-less smart diaper based on NFC technology," *IEEE Sensors J.*, vol. 19, no. 22, pp. 10848–10858, Nov. 2019.

[16] S. Chandra Kishore, K. Samikannu, R. Atchudan, S. Perumal, T. N. J. I. Edison, M. Alagan, A. K. Sundramoorthy, and Y. R. Lee, "Smartphone-operated wireless chemical sensors: A review," *Chemosensors*, vol. 10, no. 2, p. 55, Jan. 2022.

[17] R. C. Reedy and B. R. Scanlon, "Soil water content monitoring using electromagnetic induction," *J. Geotechnical Geoenvironmental Eng.*, vol. 129, no. 11, pp. 1028–1039, Nov. 2003.

[18] R. B. McCleskey, D. K. Nordstrom, J. N. Ryan, and J. W. Ball, "A new method of calculating electrical conductivity with applications to natural waters," *Geochimica et Cosmochimica Acta*, vol. 77, pp. 369–382, Jan. 2012.

[19] C. Coleman, *An Introduction to Radio Frequency Engineering*. Cambridge, U.K.: Cambridge Univ. Press, 2004.

[20] W. Olthuis, W. Streekstra, and P. Bergveld, "Theoretical and experimental determination of cell constants of planar-interdigitated electrolyte conductivity sensors," *Sens. Actuators B, Chem.*, vol. 24, nos. 1–3, pp. 252–256, Mar. 1995.

[21] S. L. Schiefelbein, N. A. Fried, K. G. Rhoads, and D. R. Sadoway, "A high-accuracy, calibration-free technique for measuring the electrical conductivity of liquids," *Rev. Scientific Instrum.*, vol. 69, no. 9, pp. 3308–3313, Sep. 1998.

[22] T. S. Light, "Temperature dependence and measurement of resistivity of pure water," *Anal. Chem.*, vol. 56, no. 7, pp. 1138–1142, Jun. 1984.

[23] R. B. McCleskey, "New method for electrical conductivity temperature compensation," *Environ. Sci. Technol.*, vol. 47, no. 17, pp. 9874–9881, Sep. 2013.

[24] M. Hayashi, "Temperature-electrical conductivity relation of water for environmental monitoring and geophysical data inversion," *Environ. Monitor. Assessment*, vol. 96, nos. 1–3, pp. 119–128, Aug. 2004.

[25] *Basics of electrochemical impedance spectroscopy*, Complex Impedance Corrosion, Gamry Instrum., Warminster, PA, USA, 2007, pp. 1–30. Accessed: Mar. 26, 2024. [Online]. Available: https://www.gamry.com/application-notes/EIS/basics-of-electrochemical-impedance-spectroscopy/

[26] S. R. Taylor and E. Gileadi, "Physical interpretation of the warburg impedance," *Corrosion*, vol. 51, no. 9, pp. 664–671, Sep. 1995.

[27] J. Braunstein and G. D. Robbing, "Electrolytic conductance measurements and capacitive balance," *J. Chem. Educ.*, vol. 48, no. 1, p. 52, Jan. 1971.

[28] E. Ferrara, L. Callegaro, and F. Durbiano, "Optimal frequency range for the measurement of AC conductivity in aqueous solutions," in *Proc. 17th IEEE Instrum. Meas. Technol. Conf.*, vol. 2, 2000, pp. 775–779.

[29] X. Li and G. C. M. Meijer, "A low-cost and accurate interface for four-electrode conductivity sensors," *IEEE Trans. Instrum. Meas.*, vol. 54, no. 6, pp. 2433–2437, Dec. 2005.
[30] A. Lazaro, M. Boada, R. Villarino, and D. Girbau, "Feasibility study on the reading of energy-harvested implanted NFC tags using mobile phones and commercial NFC IC," in *IEEE MTT-S Int. Microw. Symp. Dig.*, Dec. 2020, pp. 1–3.
[31] D. R. Muñoz and S. C. Berga, "An analog electronic interface to measure electrical conductivity in liquids," *Measurement*, vol. 38, no. 3, pp. 181–187, Oct. 2005.
[32] S Studio. *Grove-EC Sensor Kit*. Accessed: Feb. 22, 2024. [Online]. Available: https://www.seeedstudio.com/Grove-EC-Sensor-Kit-DJS-1C-Black-p-4576.html
[33] Y. Wei, J. Wang, D. Li, and Q. Ding, "Design of intelligent conductivity meter based on MSP430F149," in *Proc. Comput. Comput. Technol. Agricult. III, 3rd IFIP TC 12 Int. Conf. (CCTA)*, Beijing, China. Cham, Switzerland: Springer, 2010, pp. 240–247.
[34] E. Serrano-Finetti, C. Aliau-Bonet, O. López-Lapeña, and R. Pallàs-Areny, "Cost-effective autonomous sensor for the long-term monitoring of water electrical conductivity of crop fields," *Comput. Electron. Agricult.*, vol. 165, Oct. 2019, Art. no. 104940.
[35] H. A. Wheeler, "Simple inductance formulas for radio coils," *Proc. IRE*, vol. 16, no. 10, pp. 1398–1400, Oct. 1928.
[36] A. Lazaro, R. Villarino, M. Lazaro, N. Canellas, B. Prieto-Simon, and D. Girbau, "Battery-less NFC potentiostat for electrochemical point-of-care sensors based on COTS components," *Sensors*, vol. 22, no. 19, p. 7213, Sep. 2022.
[37] H. Zhu, S. Lai, and H. Dai, "Solutions of metal surface effect for HF RFID systems," in *Proc. Int. Conf. Wireless Commun., Netw. Mobile Comput.*, Sep. 2007, pp. 2089–2092.
[38] B. Lee, B. Kim, and S. Yang, "Enhanced loop structure of NFC antenna for mobile handset applications," *Int. J. Antennas Propag.*, vol. 2014, pp. 1–6, 2014.
[39] H. Chen and A. Zhao, "NFC antenna for portable device with metal back cover," in *Proc. IEEE Int. Symp. Antennas Propag. (APSURSI)*, Jun. 2016, pp. 1471–1472.
[40] B. Lee and F. J. Harackiewicz, "Design of a simple structured NFC loop antenna for mobile phones applications," *Prog. Electromagn. Res. C*, vol. 76, pp. 149–157, 2017.
[41] R. Bataller, J. M. Gandía, E. García-Breijo, M. Alcañiz, and J. Soto, "A study of the importance of the cell geometry in non-faradaic systems. A new definition of the cell constant for conductivity measurement," *Electrochimica Acta*, vol. 153, pp. 263–272, Jan. 2015.
[42] E. W. Rice and L. Bridgewater, Eds., *Standard Methods for the Examination of Water and Wastewater*, vol. 10. Washington, DC, USA: American Public Health Association, 2012.
[43] M. R. Spiegel, J. J. Schiller, and R. A. Srinivasan, *Schaum's Outline of Probability and Statistics*. New York, NY, USA: McGraw-Hill Education, 2013.
[44] R. R. Wolfe, S. C. Sharma, and G. E. Ward, "A method for electronic detection of bovine mastitis," *Trans. ASAE*, vol. 15, no. 3, pp. 500–503, 1972.
[45] J. L. Linzell and M. Peaker, "Efficacy of the measurement of the electrical conductivity of milk for the detection of subclinical mastitis in cows: Detection of infected cows at a single visit," *Brit. Veterinary J.*, vol. 131, no. 4, pp. 447–461, Jul. 1975. [Online]. Available: https://www.sciencedirect.com/science/article/pii/S0007193517352405

ANTONIO LAZARO (Senior Member, IEEE) was born in Lleida, Spain, in 1971. He received the M.S. and Ph.D. degrees in telecommunication engineering from Universitat Politècnica de Catalunya (UPC), Barcelona, Spain, in 1994 and 1998, respectively. Then, he joined as a Faculty Member of UPC, where he currently teaches a course on microwave circuits and antennas. Since July 2004, he has been a full-time Professor with the Department of Electronic Engineering, Universitat Rovira i Virgili (URV), Tarragona, Spain. His research interests include microwave device modeling, on-wafer noise measurements, monolithic microwave integrated circuits (MMICs), low-phase noise oscillators, MEMS, RFID, UWB, and microwave systems.

RAMON VILLARINO received the degree in telecommunications technical engineering from Ramon Llull University (URL), Barcelona, Spain, in 1994, and the degree in senior telecommunications engineering and the Ph.D. degree from Universitat Politècnica de Catalunya (UPC), Barcelona, in 2000 and 2004, respectively. From 2005 to 2006, he was a Research Associate with the Technological Telecommunications Center of Catalonia (CTTC), Barcelona. He was a Researcher and an Assistant Professor with Universitat Autònoma de Barcelona (UAB), from 2006 to 2008. Since January 2009, he has been a full-time Professor with Universitat Rovira i Virgili (URV), Tarragona, Spain. His research interests include radiometry, microwave devices, and systems based on UWB, RFIDs, and frequency-selective structures using metamaterials (MM).

MERCE PACIOS received the Ph.D. degree in chemistry from the Autonomous University of Barcelona, Spain, in 2011. Her work was based on the study of carbon nanotubes as platforms for biosensors. In 2013, she was awarded with a Marie Curie IE Fellowship at the University of Oxford, U.K. Her activities were focused on the study of 2D materials' properties and additive nanomanufacturing processes. In 2016, she joined the Catalonia Institute for Energy Research (IREC), Spain, where she worked with silicon-based nanomaterials for energy applications, such as thermoelectricity. Currently, she is with the Bioinspired Nanotechnologies Laboratory, Universitat Rovira i Virgili. Her current research interests include delivering advanced functional materials as solutions for healthcare and environmental applications. More specifically, on developing cutting-edge biosensing technology-silicon-based porous nanostructures-for early diagnosis of bovine mastitis.

MARC LAZARO was born in Tarragona, Spain, in 1995. He received the B.S. degree in industrial electronics and automation engineering and the M.S. degree in electronic systems engineering and technology (METSE) from Rovira i Virgili University, Tarragona, in 2017 and 2018, respectively, where he is currently pursuing the Ph.D. degree with the Department of Electronics. Since then, he has accumulated professional experience as a Data Acquisition Engineer and an Embedded Systems Developer. His research interests include semi-passive RFID technologies based on backscattering communication and novel applications based on millimeter wave identification (MMID).

NICOLAU CANELLAS received the Ph.D. degree from Rovira i Virgili University, Tarragona, Spain, in 2006. He started working on hardware/software co-design for biometric pattern recognition issues. In 2006, he joined the MINOS/SIPOMICS Research Group. He is currently an Associate Professor with Rovira i Virgili University. His research interests moved to the metabolomics field, where he is currently working on the development of advanced tools for 1H-NMR data analysis and signal processing and data analysis methods to facilitate the discovery of biomarkers by metabolic techniques.

DAVID GIRBAU (Senior Member, IEEE) received the B.Sc. degree in telecommunication engineering, the master's degree in electronics engineering, and the Ph.D. degree in telecommunication from Universitat Politècnica de Catalunya (UPC), Barcelona, Spain, in 1998, 2002, and 2006, respectively. From February 2001 to September 2007, he was a Research Assistant with UPC. From September 2005 to September 2007, he was a part-time Assistant Professor with Universitat Autònoma de Barcelona (UAB). Since October 2007, he has been a full-time Professor with Universitat Rovira i Virgili (URV), Tarragona, Spain. His research interests include microwave devices and systems, with an emphasis on UWB, RFIDs, RF-MEMS, and wireless sensors.

BEATRIZ PRIETO-SIMON is currently an ICREA Research Professor and a Group Leader with the Institute of Chemical Research of Catalonia. Her research interests include the multidisciplinary domain of bioinspired nanotechnologies covers the design, micro- and nanofabrication, and surface chemistry of emerging nanostructures, with the aim to integrate them into diagnostic devices fit-for-purpose. Her research aims to unveil fundamental advances in synergies at the interface of nanostructured materials and biological processes by building smart platforms based on principles found in nature. Her key research interest lies in exploiting the knowledge acquired to address diagnostic issues pointed out by clinicians and end-users to underpin technology adoption, and thus its translation from concept to application in the real world.